Nanoscale

A light-triggerable formulation to control the stability of pro-angiogenic transcription factor hypoxia inducible factor-1A (HIF-1A)

Journal:	*Nanoscale*
Manuscript ID	NR-COM-12-2019-010503.R1
Article Type:	Communication
Date Submitted by the Author:	n/a

Complete List of Authors:	Blersch, Josephine; University of Coimbra Center for Neuroscience and Cell Biology Francisco, Vitor; University of Coimbra Center for Neuroscience and Cell Biology; University of Coimbra Faculty of Medicine Rebelo, Catarina; University of Coimbra Center for Neuroscience and Cell Biology; University of Coimbra Faculty of Medicine Jiménez, Adrián; University of Coimbra Center for Neuroscience and Cell Biology Antunes, Helena; University of Coimbra Center for Neuroscience and Cell Biology; University of Coimbra Faculty of Medicine Pinto, Sandra; University of Coimbra Center for Neuroscience and Cell Biology Simoes, Susana; University of Coimbra Center for Neuroscience and Cell Biology Rai, Akhilesh; University of Coimbra Faculty of Medicine Ferreira, Lino; University of Coimbra Center for Neuroscience and Cell Biology; University of Coimbra Faculty of Medicine

Table of Contents

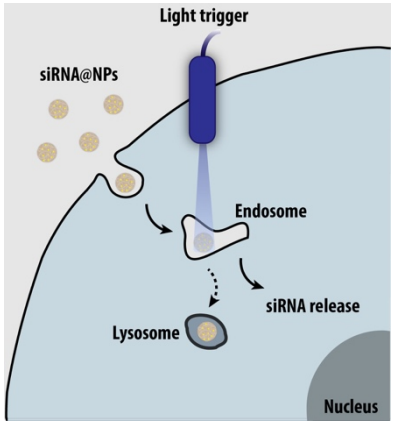

Combining nanoparticle physico-chemical diversity and light responsiveness for the delivery of siRNA to regulate transcription factor HIF-1α

A light-triggerable formulation to control the stability of pro-angiogenic transcription factor hypoxia inducible factor-1α (HIF-1α)

Josephine Blersch[1], Vitor Francisco[1,2], Catarina Rebelo[1,2], Adrian Jiménez-Balsa[1], Helena Antunes[1,2], Sandra Pinto[1], Susana Simões[1], Akhilesh Rai[2], Lino Ferreira[1,2]**

[1]Center for Neuroscience and Cell Biology, University of Coimbra, Coimbra, Portugal
[2]Faculty of Medicine, University of Coimbra, 3000-548, Coimbra, Portugal

The control of vascular remodeling mediated by transcription factor HIF-1α is critical in several diseases including cancer, retinopathies, chronic wounds, ischemic heart disease, among others. Gene silencing using small interfering RNA (siRNA) is a promising therapeutic strategy to regulate HIF-1α; however, the delivery systems developed so far have limited endothelial targeting and efficiency. Herein, we have synthesized a light-triggerable polymeric nanoparticle (NP) library composed by 110 formulations which showed variable morphology, charge and disassembly rates after UV exposure. More than 35% of the formulations of the library were more efficient in gene knockdown than siRNA delivered by a commercial transfection agent (lipofectamine RNAiMAX). The most efficient siRNA delivery formulations were tested against different cell types to identify one with preferential targeting to endothelial cells. Using a two-steps methodology, we have identified a formulation that shows exquisite targeting to endothelial cells and is able to deliver more efficiently the siRNA that modulates HIF-1α than commercial transfection agents. Overall, the strategy reported here increases the specificity in tissue regulation and the efficiency in the intracellular delivery of siRNAs.

The abnormal activation of hypoxia inducible factor-1α (HIF-1α) pathway leads to the overexpression of angiogenic growth factors that causes undesirable neovascularization in tissues such as retina and primary tumors.[1] Moreover, despite the ischemia in several diseases, HIF-1α is destabilized in diabetic wounds[2], critical limb ischemia[3] and ischemic heart disease.[4] HIF-1α is

regulated by an enzyme called prolyl hydroxylase domain protein 2 (PHD2).[1, 4] This enzyme is active in normoxia conditions and thus triggers the degradation of the transcription factor while inactive in hypoxia conditions and thus the stabilization of the transcription factor induces the expression of pro-angiogenic growth factors such as vascular endothelial growth factor (VEGF), basic fibroblast growth factor (bFGF), among others.[1, 4] The inhibition of PHD2 has been attempted with small molecules; however, these drugs have shown off-targets.[5] siRNAs have emerged as an attractive tool for regulating gene expression and thus to inhibit HIF-1α. Indeed, studies have demonstrated the inhibitory properties of PHD2 siRNA in the context of wound healing[6, 7] and cancer;[8] however, with limited efficacy and the targeting to endothelial cells, important in the context of cancer[9] and ischemic diseases,[10] was not demonstrated.

A large variety of siRNA delivery system have been developed relying on cell penetrating peptides, lipid-based formulations and polymeric NPs,[11-13] some of them identified by high-throughput screening approaches.[14-17] A limited number of these strategies have progressed to clinical trials and some of them reached the market.[18] Despite the significant progresses in the delivery of siRNA, two major issues have yet not been completely addressed: (i) limited cell targeting of the formulations increasing the concerns about potential off target effects and (ii) low endosomal escape limiting its efficacy.[19, 20] Although lipidic NPs able to release more efficiently siRNA to endothelial cells have been described,[21] the molecular mechanism is not yet known. Experimental *in vitro* data indicate that the endosomal escape of siRNA should take place during the early stages of the intracellular trafficking (minutes range after formulation uptake) to prevent their accumulation in the lysosomes.[22-24] In the current study, we hypothesize that enhanced endothelial cell targeting might be achieved by the use of NP libraries with physico-chemical diversity, being the cell targeting controlled by a combination of NP size, geometry, charge and composition. We further hypothesize that enhanced endosomal escape might be achieved by using light-triggerable formulations that are taken up by cells and disassemble rapidly (minutes range) by light releasing the siRNA.

Herein, we have designed a light-triggerable formulation that shows preferential accumulation in endothelial cells while releasing more efficiently PHD2 siRNA in cell cytoplasm than other commercial transfection agents. To identify that formulation, we have prepared a library of light-triggerable polymeric NPs for the delivery of siRNA. Then, the polymers were conjugated with a light sensitive molecule to increase their hydrophobicity as well as to confer light responsiveness properties. The conjugated polymers were then precipitated in water to form NPs and then complexed with siRNA. The NPs were characterized for their size, zeta potential, light disassembly properties, cellular internalization and gene knockdown activity. The top hits were then tested against different cell types to identify a formulation with the highest tropism to endothelial cells. Finally, the hit formulation was tested regarding its efficacy in the inhibition of endothelial cell PHD2 gene.

The library of poly(amido amine)s was prepared by Michael-type addition[22,24,25] of bisacrylamides with diamines in dimethyl sulfoxide (DMSO) for 5 days at 60 °C (**Figure 1A**). Monomers were selected based in their chemical properties (hydrophobicity/hydrophilicity, composition, structure) or by the fact that they have been used with success in previous NP libraries (**Figure 1B and 1C**). This strategy allowed us the preparation of polymers with (i) a large variety of side groups (structure: linear, ring, branched; reactivity: primary, secondary and tertiary amines; molecular weight), (ii) disulfide bonds that were relative stable in physiological conditions (pH 7.4) but likely degraded in intracellular reductive environments and (iii) different solubility in aqueous solution. In the final stage of reaction, an excess of the amine monomer was added to ensure that acrylamide end groups were capped with amines in order to increase transfection efficiency.[26] To confer light responsiveness properties to the polymers, a light sensitive pendant group was attached to the polymer backbone. Therefore, the polymer library was reacted with 4,5-dimethoxy-2-nitrobenzyl chloroformate (NVOC), in the presence of trimethylamine as a catalyst. NVOC was selected because it responds rapidly to UV/blue light and the degradation products are relatively non-cytotoxic.[27]

To validate the overall synthetic strategy, we randomly selected one polymer and characterized it by NMR (**Figure S1A**). ^{1}H-NMR spectrum of A4 showed the absence of acrylate protons (5.5 to 7.0 ppm) indicating complete reaction of the acrylamide with the amines. Moreover, the spectrum of A4 showed the expected peaks of NVOC protons at δ 7.9, 7.7, 5.1 and 3.8-3.9 ppm. Successful conjugation of A4 with NVOC was also confirmed by spectrophotometry (**Figure S1B**). As expected, the absorbance spectrum of A4 showed an absorbance maximum at 354 nm after NVOC conjugation. After UV irradiation of the polymer for 10 min, there is the cleavage of the NVOC moiety of the polymer (approximately 50%; for a polymer with an experimental degree of substitution (DS_{exp}) of 20%) and the consequent decrease in the absorbance at 354 nm. A4 NPs were obtained by nanoprecipitation of A4 polymer conjugated with NVOC in aqueous solution, followed by the addition of zinc sulphate to stabilize the NPs.[28] To form light-responsive NPs, a compromise between hydrophobicity (which impacts in NP yield by the nanoprecipitation process) and light-responsiveness (high conjugation of the polymer with NVOC slows down the NP photo-disassembly) process should be optimized. To address this issue, A4 polymer was conjugated with three different molar ratios of NVOC: diamine (**Figure S1C**) and then the individual polymers precipitated in aqueous solution. The NP efficiency for A4 with a DS_{exp} of NVOC of 20% was 16% (i.e., percentage of mass recovered from the initial monomers used for polymer synthesis and derivatization). After activation with UV light, NVOC is cleaved from the polymer, which changes the hydrophobic-hydrophilic balance in the NPs resulting in its disassembly. This response is expressed in the percentage count decrease of NPs, as monitored by dynamic light scattering (DLS). The NPs formed by polymers with a DS_{exp} of 20% (i.e. the molar ratio of NVOC: diamine was 1:5) showed the highest NPs count decrease after UV irradiation (**Figure S2**). Therefore, this molar ratio was adopted to synthesize the library with 110 possible polymers.

Next, we have synthesized the NP library and characterize the properties of NPs according to size, zeta potential and light responsiveness. Most of the polymers (90%) were able to form NPs by nanoprecipitation, while 10% were either soluble in water or formed aggregates that rapidly

flocculated and deposited. The high-water solubility of some polymers was likely due to the low conjugation of the polymer with NVOC because of the low amine groups in the polymer. Next, we determined the NP formation efficiency taking into account the mass of monomers used for the synthesis and conjugation of the polymers and the resulting NP mass after freeze-drying (**Figure S3A**). The median NP formation efficiency was 27 ± 15%. The NPs were then characterized by DLS, to obtain NPs size (**Figure S3B**) and zeta potential (**Figures S3C and S3D**). Ninety percent of NPs had a size between 50 and 500 nm, while 65% of the NPs showed positive charge (zeta potential>10 mV). NPs composed by crosslinkers A and C had narrow size distribution and highly positive zeta potential. NPs composed by diamines 5-8 and 15-18 had the highest positive zeta potential. Next, we evaluated the light responsiveness of the NP library (**Figure S3E**). More than 90% of the formulations were sensitive to UV irradiation. Approximately 79% of the formulations had a 50% decrease after 10 min of UV irradiation. The light responsiveness of the NPs formulations was likely influenced by the presence of aromatic moieties, the hydrophobicity of the polymer before NVOC conjugation, among others. It was largely independent of the characteristics of the crosslinker but dependent in the diamines composition, since aromatic diamines (12-15 and 23), negatively affected the light-response of the formulation.

To evaluate the capacity of NPs to complex siRNA, each NP formulation was mixed with a GFP-silencing siRNA for 2 h to promote electrostatic interactions. The ratio siRNA to NP was optimized to yield the highest knockdown efficiency in HeLa-GFP cells, being the ratio siRNA:NP of 1:50 (w/w) the most effective (**Figure S4**). This ratio is a compromise between NP charge (accounting for cell uptake) and siRNA concentration (accounting for bioactivity). Therefore, all the subsequent steps were done with this siRNA:NP ratio. Next, we quantified the complexation efficiency of siRNA with the library of NPs by fluorescence spectroscopy. NPs were centrifuged after the complexation and the concentration of labelled siRNA (tagged with a Cy5 dye) quantified in the supernatant. For all the formulations, the median efficiency was 70±27%, being 40% of the formulations able to complex more than 75% of the siRNA (**Figure S5A**). The most effective

formulations in binding siRNA were composed by crosslinker A, C or E and diamines with higher aliphatic contribution (2, 3, 11, 16, 21, 22) or high amine content (4, 5, 6, 7, 11). These results indicated that the binding of siRNA was not only dependent on positive zeta-potential (mostly caused by amines) but also by the presence of aliphatic domains.

After demonstrating the capacity of NPs to complex siRNA and disassemble after UV exposure, we evaluated NP@siRNA mediated gene knockdown upon light activation using siRNA against eGFP in HeLa-GFP cells. For that purpose, cells were transfected with NP@siRNA (siRNA:NP 1:50 (w/w), 20 μg/mL) complexes for 10 min (**Figure S4B**), washed to remove non-internalized complexes, light-activated for 10 min and cultured for additional 48 h. Non-treated HeLa-GFP and HeLa-GFP cells transfected with lipofectamine RNAiMAX complexed with siRNA were used as controls. Cell viability (evaluated by propidium iodide (PI) staining), NP internalization (evaluated by the Cy5 tag of the siRNA) and GFP knockdown results were obtained by high-content microscopy analyses. GFP knockdown was calculated as percentage decrease of GFP fluorescence signal relative to non-treated HeLa-GFP cells and HeLa-GFP cells transfected with lipofectamine complexed with siRNA. No significant impact in cell viability was observed for all the NPs of the library (cell viability>90%) (**Figure S5B**). NP formulations were internalized by HeLa cells and accumulated in the cell cytoplasm for at least 48 h (**Figure S5C**). To further demonstrate the delivery of siRNA to the cell cytoplasm, we have transfected HeLa cells for 10 min with C11@siRNA-Cy5 or with Lipo@siRNA-Cy5 followed by irradiation or not with UV light (**Figure S6**). The intracellular trafficking of the formulations was monitored by confocal microscopy using a general endolysosomal staining (LysoTracker). The results showed lower co-localization of C11@siRNA-Cy5 with endolysosomes after irradiation than before irradiation indicating that the rapid NP disassembly favored the escape of siRNA from the endolysosomal compartment (**Figure S6**). Importantly, more than 35% of the formulations were more efficient in GFP knockdown than lipofectamine RNAiMAX (fold increase>1) (**Figure 1D**). Formulations containing crosslinkers A, C or E and diamines 1, 4-7 or 10-11 showed the highest GFP knockdown activity. Five formulations (C11, A10, A1, A9 and E1)

showed more than 3-fold increase relative to lipofectamine RNAiMAX in GFP knockdown and were selected for further studies.

The uptake of NPs by cells is dependent on multiple factors such as NP size,[29] NP shape,[30] NP surface chemistry,[31-33] and the type of cell and its machinery, since each cell type may internalize the same NP by different endocytic pathways. For example, polystyrene NPs are highly taken up by endothelial and hepatocyte cells and less by macrophages and epithelial cells.[34] To identify NPs able to target more preferentially endothelial cells, we evaluated NP@siRNA-Cy5 internalization in different type of cells through colocalization with the endolysosomal compartment (Lysotracker) by confocal microscopy. Because one of the potential applications of these light-triggerable NPs is for skin applications[35] we have chosen human keratinocytes, dermal fibroblasts and endothelial cells as cell models to investigate endothelial cell-specific NP uptake. Six efficient gene silencing formulations (A1, A9, A10, C11, E1, E2) and one non-efficient formulation (E21, which presented lower knockdown activity than lipofectamine) were chosen to assess cell uptake (**Figure 2**). Cells were transfected either with NP@siRNA-Cy5 or Lipo@siRNA-Cy5 for 1 h, washed to remove the NPs that were not internalized, and analyzed by confocal microscopy. From all the formulations tested, C11 formulation was the highest taken up by endothelial cells while showing low uptake by keratinocytes and fibroblasts. Based in the high efficacy of C11 to transfect endothelial cells and in the knockdown activity demonstrated in HeLa-GFP cells, this formulation was selected for subsequent studies. Initially, the physical-chemical properties of C11 formulation were investigated. The polymer had a DS_{exp} of 24%, as measured by ^{1}H-NMR (**Figure S7A**), a Mw of 12.700 Da, as evaluated by GPC, and was responsive to UV irradiation, as measured by spectrophotometry (**Figure S7B**). When C11 was complexed with siRNA yielded NPs with an average diameter of ~60 nm and a zeta potential of 13.9 ± 1.2 mV, as demonstrated by DLS and TEM analysis (**Figure S7C and D**). The NPs disassembled after UV (365 nm, 10 min) light irradiation (more than 80%) (**Figure S7E**) due to the cleavage of NVOC moiety and the disruption of the hydrophobic/hydrophilic balance in

the NP, and release the siRNA (**Figure S7F**). We also investigated whether UV light could cross skin tissue and trigger the release of siRNA from the C11 formulation. Indeed, UV radiation is able to cross the skin tissue at the necessary level to disassemble the NP formulation (**Figure S8**).

To demonstrate the utility of C11, we have complexed the NP with PHD2 siRNA and tested the formulation in endothelial cells. It has been shown that HIF-1α stabilization in endothelial cells by PHD2 inhibition induces VEGF upregulation, which leads to proliferation and migration of the cells (**Figure 3A**).[36-38] We have performed the experiments in normoxia since mRNA and protein expression of HIF-1α was higher in normoxia than in hypoxia after cell transfection with shPHD2.[39] The effect of UV in cell viability and activity was initially evaluated. Our results showed no influence in viability, proliferation or migration in cells exposed to UV light (365 nm, 10 min) relatively to non-exposed cells (**Figure S9**). Next, we evaluated cell migration and proliferation after transfection with C11@PHD2 NPs. Cells were transfected for 12 h with C11@PHD2 NPs, activated or not with a UV light for 10 min, and cell migration evaluated in a wounded monolayer of endothelial cells (**Figure 3B**). Our qRT-PCR analyses indicate that PHD2 mRNA available in the cytoplasm was lower in cells transfected with C11@PHD2 NPs and activated by light as result of the inhibition of the siRNA (**Figure 3C**). Endothelial cell migration was significantly increased when cells were treated with C11@PHD2 NPs after light activation as compared to cells treated with C11@PHD2 NPs without light activation or non-treated cells (**Figures 3D and 3E**). Therefore, our results indicate that C11@PHD2 NPs efficiently delivered the siRNA to endothelial cells and the exposure to light improved PHD2 siRNA release from C11 NPs. Next, we evaluated the biological activity of siRNA delivered by C11@PHD2 NPs in a cell proliferation assay (**Figure 3B and 3F**). Cells were transfected for 12 h with C11@PHD2 NPs, activated or not with a UV light for 10 min, and cell proliferation evaluated for 36 h by cell counting using a high-content microscope. Our results indicate that cells transfected with C11@PHD2 NPs and then activated by light proliferated at higher extent than cells treated with C11@PHD2 NPs but not exposed to light. Although C11 formulation has

disulfide bonds incorporated in polymer backbone (monomer C), and therefore can be cleaved by intracellular glutathione, the results show that light activation is required to maximize its biological effect (cell migration and proliferation).

In conclusion, we have developed a formulation that has preferential accumulation in endothelial cells and release more efficiently siRNA in the cell cytoplasm than a conventional transfection agent. The formulation has been identified by a two-step methodology comprising a high-throughput screening of a new light-triggerable NP library and then testing the top hits against several cell types to identify a formulation that has more accumulation in endothelial cells. The NP library proposed here had higher gene knock-down activity (30% of the formulations showed higher knock-down activity than lipofectamine) than another NP library (10% of the formulations showed higher knock-down activity than lipofectamine) recently reported by us.[40] In this study, the light-responsive library of NPs was based in a simple principle, i.e., conjugation of a light-sensitive pendant molecule (NVOC) to polymers synthesized by high-throughput while in the previous study we have incorporated a light-responsive monomer in the core of the polymer. In addition, using the current synthetic scheme we could identify formulations with higher endothelial cell accumulation than the top hits tested in the previous study. It is currently not known the factors that mediate endothelial cell targeting and future studies should address this issue. It is possible that a combination of NP cell internalization, kinetics of NP disassembly and intrinsic NP physico-chemical properties may account for the differential NP uptake and gene knockdown activity among formulations. The best formulation identified in this study (C11) shows a balance between these 3 properties. Importantly, our results showed that the rapid disassembly (in the first 10 min after transfection) of formulations after cell transfection enhanced their gene knockdown activity. Future studies should evaluate the *in vivo* efficacy of the current formulation. Overall, our results report a new strategy to identify formulations for efficient endothelial RNA delivery and specifically to inhibit the activity of PHD2, an enzyme that controls the stability of HIF-1α.

Supporting Information

Electronic supporting information (ESI) available: Experimental protocols relative to polymer and nanoparticle synthesis and characterization, high-throughput screening and cell internalization. Data relative to NPs characterization, light responsiveness, uptake and endosomal escape.

Conflict of Interest

There are no conflicts to declare.

Acknowledgements

The authors would like to thank the financial support of ERA Chair project (ERA@UC, ref:669088) through EU Horizon 2020 program, the POCI-01-0145-FEDER-016390 (acronym: CANCEL STEM), POCI-01-0145-FEDER-029414 (acronym: LIghtBRARY), POCI-01-0145-FEDER-029229 (acronym: Aging-Model) and UID/NEU/04539/2019 projects through Compete 2020 and FCT programs.

References

1. G. L. Semenza, *Cell*, 2012, **148**, 399-408.
2. I. R. Botusan, V. G. Sunkari, O. Savu, A. I. Catrina, J. Grunler, S. Lindberg, T. Pereira, S. Yla-Herttuala, L. Poellinger, K. Brismar and S. B. Catrina, *Proc Natl Acad Sci U S A*, 2008, **105**, 19426-19431.
3. K. Sarkar, K. Fox-Talbot, C. Steenbergen, M. Bosch-Marce and G. L. Semenza, *Proc Natl Acad Sci U S A*, 2009, **106**, 18769-18774.
4. G. L. Semenza, *Annu Rev Physiol*, 2014, **76**, 39-56.
5. P. Fraisl, J. Aragones and P. Carmeliet, *Nat Rev Drug Discov*, 2009, **8**, 139-152.
6. J. R. Martin, C. E. Nelson, M. K. Gupta, F. Yu, S. M. Sarett, K. M. Hocking, A. C. Pollins, L. B. Nanney, J. M. Davidson, S. A. Guelcher and C. L. Duvall, *Adv Healthc Mater*, 2016, **5**, 2751-2757.
7. C. E. Nelson, A. J. Kim, E. J. Adolph, M. K. Gupta, F. Yu, K. M. Hocking, J. M. Davidson, S. A. Guelcher and C. L. Duvall, *Adv Mater*, 2014, **26**, 607-614, 506.
8. M. R. Bordoli, D. P. Stiehl, L. Borsig, G. Kristiansen, S. Hausladen, P. Schraml, R. H. Wenger and G. Camenisch, *Oncogene*, 2011, **30**, 548-560.
9. M. Mazzone, D. Dettori, R. L. de Oliveira, S. Loges, T. Schmidt, B. Jonckx, Y. M. Tian, A. A. Lanahan, P. Pollard, C. R. de Almodovar, F. De Smet, S. Vinckier, J. Aragones, K. Debackere, A. Luttun, S. Wyns, B. Jordan, A. Pisacane, B. Gallez, M. G. Lampugnani, E. Dejana, M. Simons, P. Ratcliffe, P. Maxwell and P. Carmeliet, *Cell*, 2009, **136**, 839-851.
10. B. W. Wong, E. Marsch, L. Treps, M. Baes and P. Carmeliet, *EMBO J*, 2017, **36**, 2187-2203.
11. J. B. Miller and D. J. Siegwart, *Nano Research*, 2018, **11**, 5310-5337.
12. R. Kanasty, J. R. Dorkin, A. Vegas and D. Anderson, *Nat Mater*, 2013, **12**, 967-977.
13. R. S. Shukla, B. Qin and K. Cheng, *Mol Pharm*, 2014, **11**, 3395-3408.
14. A. Akinc, A. Zumbuehl, M. Goldberg, E. S. Leshchiner, V. Busini, N. Hossain, S. A. Bacallado, D. N. Nguyen, J. Fuller, R. Alvarez, A. Borodovsky, T. Borland, R. Constien, A. de Fougerolles, J. R. Dorkin, K. Narayanannair Jayaprakash, M. Jayaraman, M. John, V. Koteliansky, M. Manoharan, L. Nechev, J. Qin, T. Racie, D. Raitcheva, K. G. Rajeev, D. W. Sah, J. Soutschek, I. Toudjarska, H. P. Vornlocher, T. S. Zimmermann, R. Langer and D. G. Anderson, *Nat Biotechnol*, 2008, **26**, 561-569.
15. K. T. Love, K. P. Mahon, C. G. Levins, K. A. Whitehead, W. Querbes, J. R. Dorkin, J. Qin, W. Cantley, L. L. Qin, T. Racie, M. Frank-Kamenetsky, K. N. Yip, R. Alvarez, D. W. Sah, A. de

Fougerolles, K. Fitzgerald, V. Koteliansky, A. Akinc, R. Langer and D. G. Anderson, *Proc Natl Acad Sci U S A*, 2010, **107**, 1864-1869.
16. K. P. Mahon, K. T. Love, K. A. Whitehead, J. Qin, A. Akinc, E. Leshchiner, I. Leshchiner, R. Langer and D. G. Anderson, *Bioconjug Chem*, 2010, **21**, 1448-1454.
17. K. A. Whitehead, G. Sahay, G. Z. Li, K. T. Love, C. A. Alabi, M. Ma, C. Zurenko, W. Querbes, R. S. Langer and D. G. Anderson, *Mol Ther*, 2011, **19**, 1688-1694.
18. H. J. Kim, A. Kim, K. Miyata and K. Kataoka, *Adv Drug Deliv Rev*, 2016, **104**, 61-77.
19. *EBioMedicine*, 2018, **34**, 1.
20. P. Lonn, A. D. Kacsinta, X. S. Cui, A. S. Hamil, M. Kaulich, K. Gogoi and S. F. Dowdy, *Sci Rep*, 2016, **6**, 32301.
21. J. E. Dahlman, C. Barnes, O. Khan, A. Thiriot, S. Jhunjunwala, T. E. Shaw, Y. Xing, H. B. Sager, G. Sahay, L. Speciner, A. Bader, R. L. Bogorad, H. Yin, T. Racie, Y. Dong, S. Jiang, D. Seedorf, A. Dave, K. S. Sandu, M. J. Webber, T. Novobrantseva, V. M. Ruda, A. K. R. Lytton-Jean, C. G. Levins, B. Kalish, D. K. Mudge, M. Perez, L. Abezgauz, P. Dutta, L. Smith, K. Charisse, M. W. Kieran, K. Fitzgerald, M. Nahrendorf, D. Danino, R. M. Tuder, U. H. von Andrian, A. Akinc, A. Schroeder, D. Panigrahy, V. Kotelianski, R. Langer and D. G. Anderson, *Nat Nanotechnol*, 2014, **9**, 648-655.
22. G. Sahay, W. Querbes, C. Alabi, A. Eltoukhy, S. Sarkar, C. Zurenko, E. Karagiannis, K. Love, D. Chen, R. Zoncu, Y. Buganim, A. Schroeder, R. Langer and D. G. Anderson, *Nat Biotechnol*, 2013, **31**, 653-658.
23. J. Gilleron, W. Querbes, A. Zeigerer, A. Borodovsky, G. Marsico, U. Schubert, K. Manygoats, S. Seifert, C. Andree, M. Stoter, H. Epstein-Barash, L. Zhang, V. Koteliansky, K. Fitzgerald, E. Fava, M. Bickle, Y. Kalaidzidis, A. Akinc, M. Maier and M. Zerial, *Nat Biotechnol*, 2013, **31**, 638-646.
24. A. Wittrup, A. Ai, X. Liu, P. Hamar, R. Trifonova, K. Charisse, M. Manoharan, T. Kirchhausen and J. Lieberman, *Nat Biotechnol*, 2015, **33**, 870-876.
25. K. L. Kozielski, S. Y. Tzeng, B. A. De Mendoza and J. J. Green, *ACS Nano*, 2014, **8**, 3232-3241.
26. A. Akinc, D. G. Anderson, D. M. Lynn and R. Langer, *Bioconjug Chem*, 2003, **14**, 979-988.
27. T. Dvir, M. R. Banghart, B. P. Timko, R. Langer and D. S. Kohane, *Nano Lett*, 2010, **10**, 250-254.
28. W. Tiyaboonchai, J. Woiszwillo and C. R. Middaugh, *Journal of Pharmaceutical Sciences*, 2001, **90**.
29. S. Zhang, J. Li, G. Lykotrafitis, G. Bao and S. Suresh, *Adv Mater*, 2009, **21**, 419-424.
30. S. Venkataraman, J. L. Hedrick, Z. Y. Ong, C. Yang, P. L. Ee, P. T. Hammond and Y. Y. Yang, *Adv Drug Deliv Rev*, 2011, **63**, 1228-1246.
31. N. Oh and J. H. Park, *Int J Nanomedicine*, 2014, **9 Suppl 1**, 51-63.
32. L. Y. Chou, K. Ming and W. C. Chan, *Chem Soc Rev*, 2011, **40**, 233-245.
33. C. D. Walkey, J. B. Olsen, H. Guo, A. Emili and W. C. Chan, *J Am Chem Soc*, 2012, **134**, 2139-2147.
34. T. Xia, M. Kovochich, M. Liong, J. I. Zink and A. E. Nel, *ACS Nano*, 2008, **2**, 85-96.
35. M. M. Lino, S. Simoes, A. Vilaca, H. Antunes, A. Zonari and L. Ferreira, *ACS Nano*, 2018, **12**, 5207-5220.
36. J. A. Forsythe, B. H. Jiang, N. V. Iyer, F. Agani, S. W. Leung, R. D. Koos and G. L. Semenza, *Mol Cell Biol*, 1996, **16**, 4604-4613.
37. P. Carmeliet, Y. Dor, J. M. Herbert, D. Fukumura, K. Brusselmans, M. Dewerchin, M. Neeman, F. Bono, R. Abramovitch, P. Maxwell, C. J. Koch, P. Ratcliffe, L. Moons, R. K. Jain, D. Collen and E. Keshert, *Nature*, 1998, **394**, 485-490.
38. H. E. Ryan, J. Lo and R. S. Johnson, *EMBO J*, 1998, **17**, 3005-3015.

39. L. Zhang, Z. Sun, P. Ren, R. J. Lee, G. Xiang, Q. Lv, W. Han, J. Wang, S. Ge and M. Xie, *PLoS One*, 2015, **10**, e0134629.
40. J. Blersch, V. Francisco, C. Rebelo, A. Jimenez-Balsa, H. Antunes, C. Gonzato, S. Pinto, S. Simoes, K. Liedl, K. Haupt and L. S. Ferreira, *Angew Chem Int Ed Engl*, 2019, DOI: 10.1002/anie.201911398.
41. B. L. Krock, N. Skuli and M. C. Simon, *Genes Cancer*, 2011, **2**, 1117-1133.
42. L. A. van Meeteren and P. ten Dijke, *Cell Tissue Res*, 2012, **347**, 177-186.
43. G. Pintucci, D. Moscatelli, F. Saponara, P. R. Biernacki, F. G. Baumann, C. Bizekis, A. C. Galloway, C. Basilico and P. Mignatti, *FASEB J*, 2002, **16**, 598-600.
44. M. Calvani, A. Rapisarda, B. Uranchimeg, R. H. Shoemaker and G. Melillo, *Blood*, 2006, **107**, 2705-2712.

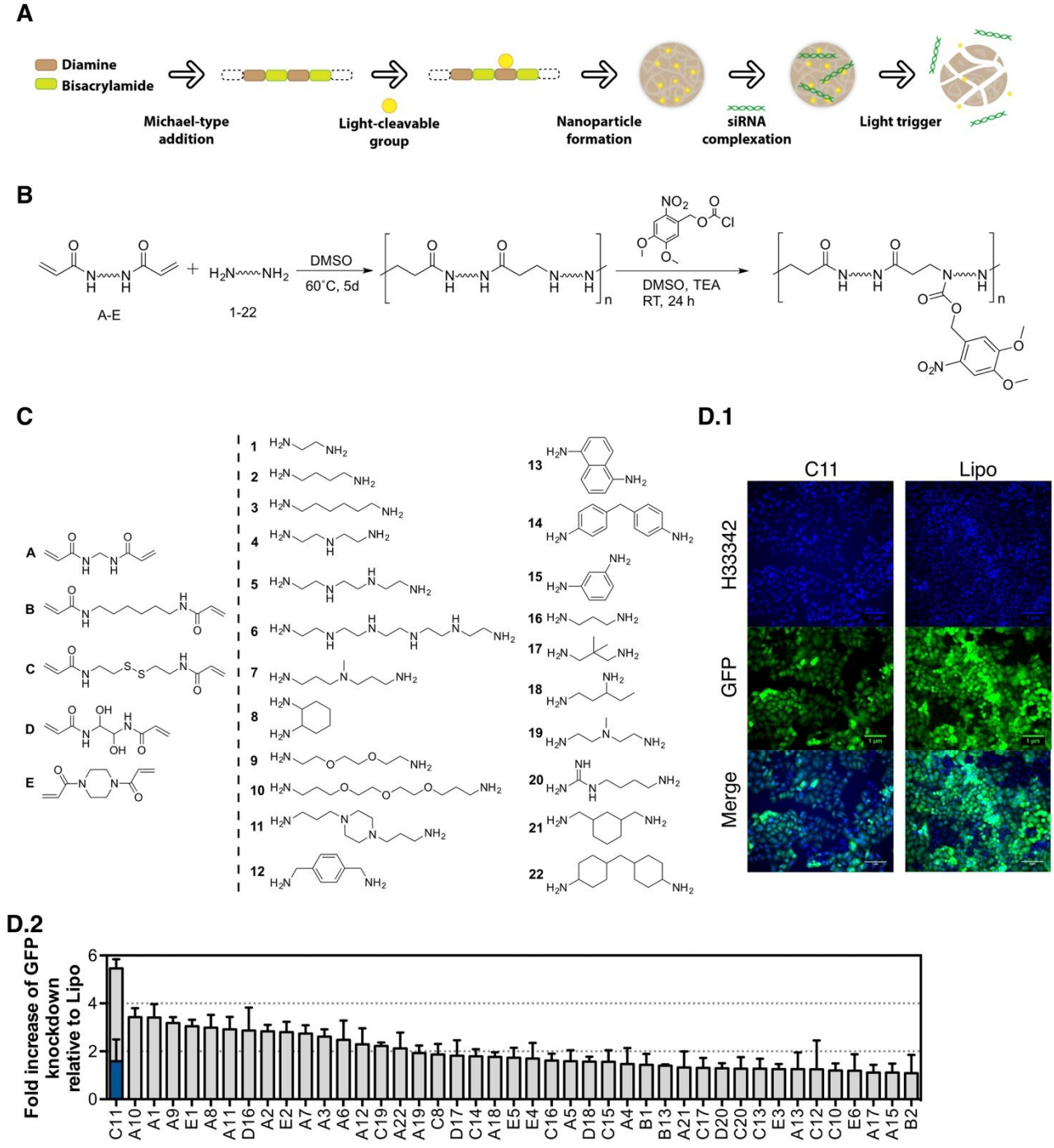

Figure 1. Light-activatable NP library and gene knockdown activity. (A) Scheme illustrating the formation of light-activatable polymers and formation of nanoparticles. (B) Reaction scheme for the combinatorial synthesis of the poly(amido amine)s, followed by the conjugation of NVOC. The mechanism of photocleavage is also presented. (C) Monomers used for the synthesis of the library: bisacrylamides (A-E) and diamines (1-22). (D.1) Gene knockdown in HeLa-GFP cells after transfection with C11 formulation containing a siRNA against GFP. Bar corresponds to 1 μm. (D.2) Gene silencing efficacy of the 43 best NP formulations. Efficacy was measured as fold increase GFP knockdown relative to Lipofectamine RNAiMAX (Lipo), 48 h post transfection. HeLa-GFP cells were transfected with 20 μg/ml NP-siRNA complexes (targeting GFP) for 10 min and activated for 10 min with UV light. The blue bar shows GFP knockdown of the best formulation without UV activation. Results are expressed as Mean ± SEM (n = 3).

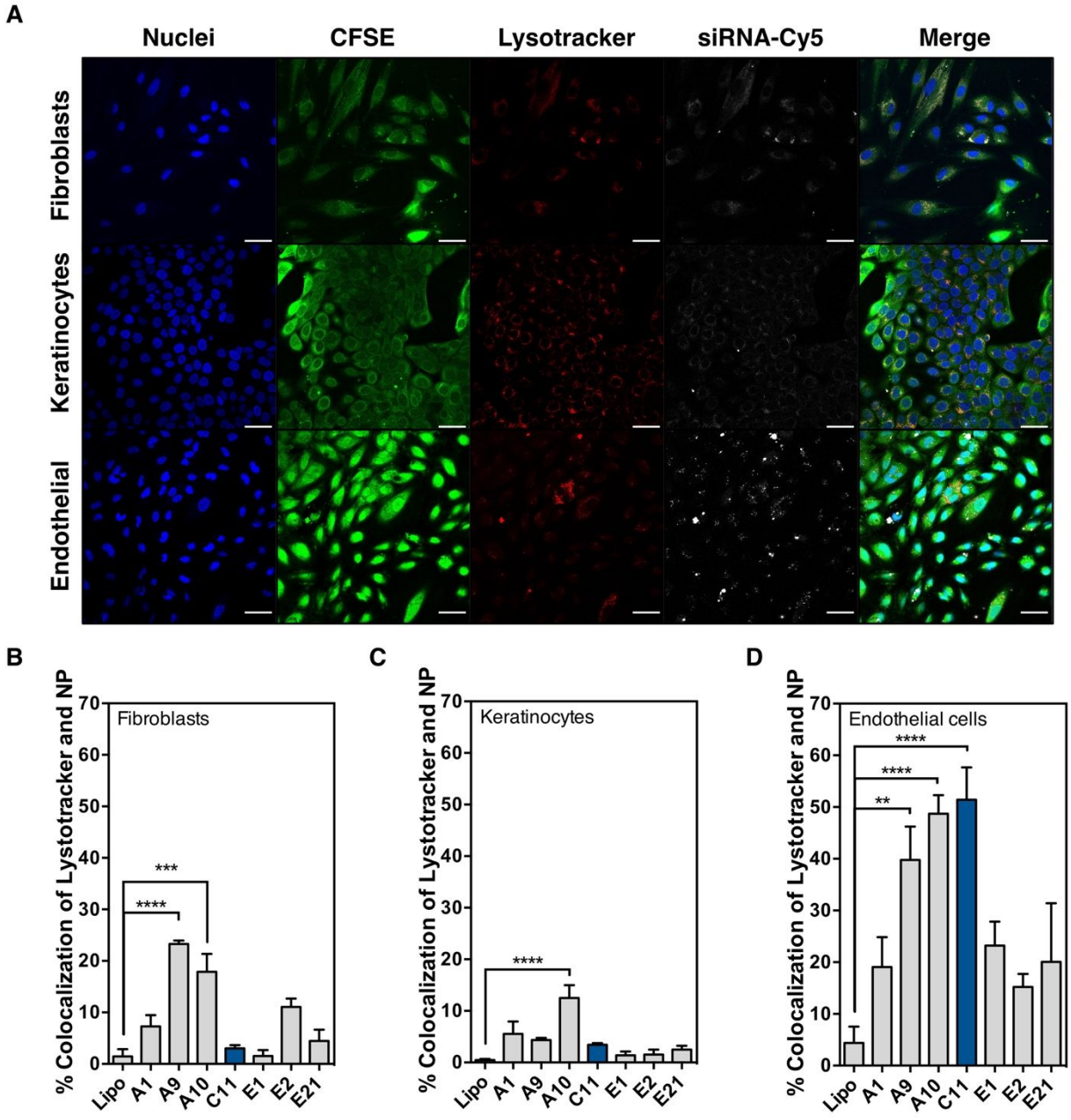

Figure 2. NP internalisation studies in human skin cells. (A) Representative images from confocal microscopy showing colocalization of C11@siRNA-Cy5 with Lysotracker red (endolysosomal compartment) in the three cell types. Scale bar corresponds to 50 µm. Human fibroblasts (B), keratinocytes (C) and endothelial cells (D) were used for internalisation studies. The following formulations have been tested: (i) high gene silencing formulations (six) identified in the high-throughput screening (A1, A9, A10, C11, E1, E2), (ii) lipofectamine RNAiMAX (Lipo; positive control) and (iii) a low gene silencing formulation (E21, negative control). Cells were transfected for 1 h with NP@siRNA-Cy5 (20 µg/mL) complexes, washed to remove non-internalised NPs, stained (cell cytoplasm with CFSE; endolysosomal compartment with Lysotracker Red; cell nuclei with H33342) and analysed by confocal microscopy using a 40x objective. Internalisation was quantified through colocalization of siRNA-Cy5 with Lysotracker red. Results are represented as Mean ± SEM (n=2 independent samples, 3-9 microscope fields per independent sample). Statistical analyses were performed by One-Way Anova followed by a Bonferroni multi-comparison test (**P<0.01; ***P<0.001; ****P<0.0001) against Lipo.

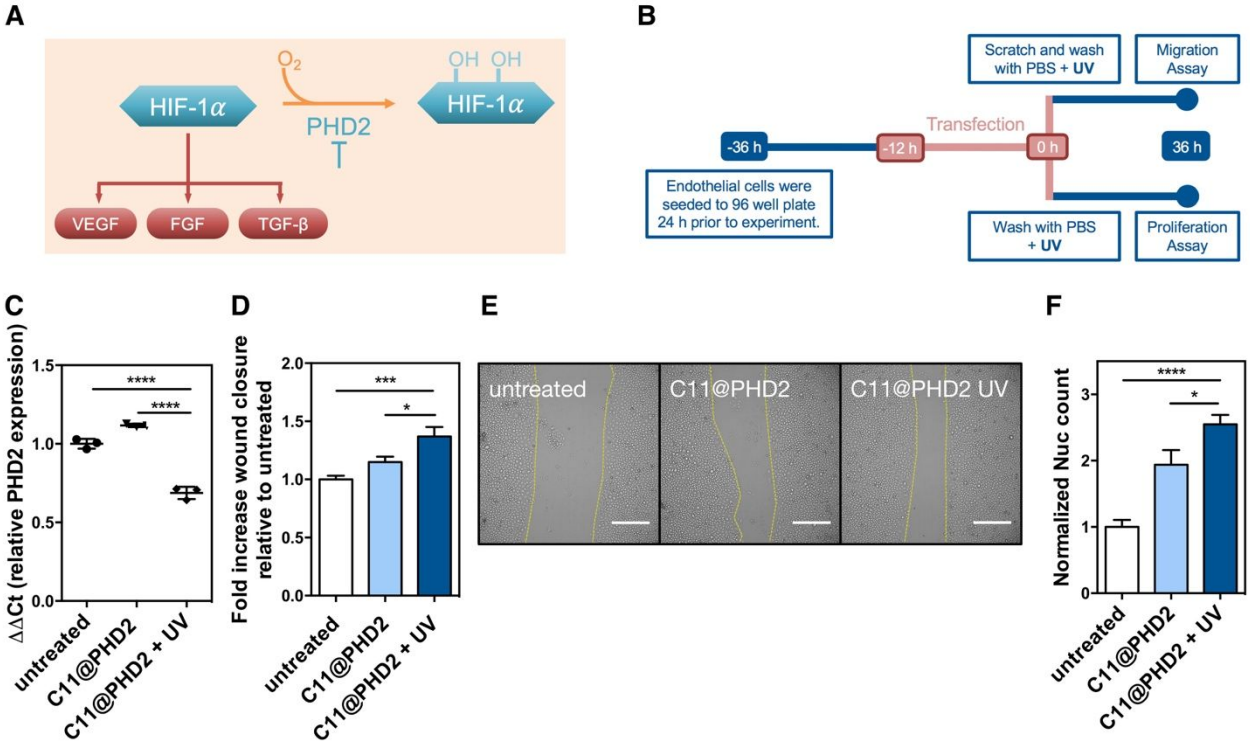

Figure 3. Bioactivity of C11@PHD2 NPs in endothelial cells. (A) Stabilization of HIF-1α by siRNA silencing PHD2 can be used as therapeutic strategy to control endothelial cell proliferation and migration, by the upregulation of VEGF and TGF-β growth factors.[41-44] (B) Schematic representation of the experimental protocol for the migration and proliferation assays. Endothelial cells were grown to confluence and transfected with C11@PHD2 for 12 h. In the migration assay, non-internalised complexes were washed, the cell monolayer was wounded with a pipette tip and irradiated or not with UV light (365 nm, 10 min, 1 mW/cm^2). Cell migration in the wounded area was monitored by high content imaging. In the proliferation assay, non-internalised complexes were removed, cells were either or not irradiated with a UV light, and then cultured for additional 36 h. (C) Cells were harvested 24 h post-transfection and evaluated for PHD2 mRNA expression by qRT-PCR analyses and expressed relatively to GAPDH mRNA. Results are presented as Mean ± SEM (n=3). (D) Relative scratch closure 36 h post wounding. Wound area was quantified in ImageJ and normalised to the initial wound area. Results are presented as Mean ± SEM (n = 3-8 wells). (E) Representative images of wounds 36 h post scratch. Scale bar corresponds to 50 µm. (F) Cell proliferation at 36 h post transfection. Nuclei were stained with H33342 and analysed by high content imaging. Relative nucleus count is presented as Mean ± SEM (n = 3-6). All Statistical analyses were performed using One-Way Anova followed by a Tukey post-test (*P<0.05; *** P<0.001; ****P<0.0001).

Supporting Information

A light-triggerable formulation to control the stability of pro-angiogenic transcription factor hypoxia inducible factor-1α (HIF-1α)

Josephine Blersch[1], Vitor Francisco[1,2]*, Catarina Rebelo[1,2], Adrian Jiménez-Balsa[1], Helena Antunes[1,2], Sandra Pinto[1], Susana Simões[1], Akhilesh Rai[2], Lino Ferreira[1,2]*

MATERIALS and METHODS

Synthesis of polymers. The library of poly (amido amine)s with light-cleavable moiety (NVOC) was synthesized via Michael addition reaction. Prior to synthesis, diamines (1-22), bisacrylamides A-E were diluted to 1.6 M in anhydrous DMSO (Sigma-Aldrich). Specifications of all monomers can be found in supplementary Table 1. After designing the plate layout for the 110 combinations between monomers A-E and 1-22, 100 µL aliquots of bisacrylamides and 100 µL aliquots of diamines were added to each well of a 96-deepwell plate (polypropylene (PP), VWR). The plates were sealed with aluminum foil and incubated for reaction at 60 ºC shaking for five days on an orbital shaker (250 rpm). Polymers were finally end capped with 20% molar excess (10 µL to 100 µL reaction volume) of the respective diamine 1-22 for 2 h (60ºC, 250 rpm). Next, the polymers were functionalized with 4,5-dimethoxy-2-nitrobenzyl chloroformate (NVOC, Sigma-Aldrich) in the presence of triethylamine (10% molar ratio, Sigma-Aldrich). The reaction was performed overnight under shaking at room temperature. Finally, the plates were stored at 4ºC until usage.

Determination of the best photocleavable group ratio in poly(amido amine)s. To optimize the amount of the photocleavable group in the poly(amido amine), ratios of 1:4, 1:8 and 1:12 of NVOC to diamine were used in the synthesis of A4 polymer. To obtain the degree of substitution of NVOC in the polymer, A4 was purified by precipitation in water, lyophilized, resuspended in DMSO-d_6 and analyzed by ^{1}H-NMR (Bruker Avance III 400 MHz) relative to TMS. After preparation of

nanoparticle with the polymers with different NVOC ratio, size and count decrease of the nanoparticles before and after UV irradiation (10 min, 365 nm, 100 mW/cm^2) were measured by DLS.

Evaluation of the best ratio siRNA:NP and transfection time in the gene knockdown efficiency. siRNA:NP ratio was optimized with formulation A4 to maximize GFP knockdown. A suspension of A4 NPs (200 µg/mL) was complexed for 2 h with siRNA against GFP in ratios of 1:12.5, 1:25 and 1:50 (w/w) in nuclease free sterile water under shaking on an orbital shaker (250 rpm) at room temperature. To bioactivity of the complexes were evaluated in HeLa-GFP cells which were seeded at a density of 40.000 cells/mL for 24 h prior the experiment. Cells were transfected for 4 h with NP@siRNA complexes (20 µg/mL) in starvation (DMEM), washed, fresh medium with reduced serum (DMEM, 5% FBS, 0.5% PenStrep) added and cultured for additional 48 h. After 48 h, cells were stained with H33342 and PI (both 0.25 µg/mL) and analyzed by fluorescence microscopy on a high-content microscope (In Cell Analyzer 2200). The quantification of cell viability and GFP knockdown is described in high content imaging section below.

The transfection time was optimized to identify a time relatively short that could lead to significant gene knockdown. In this way, cells were transfected with NP@siRNA complexes (20 µg/mL; 1:50 siRNA:NP (w/w)) from 10 min to 4 h. After a washing step, cells were cultured in medium with reduced serum (DMEM, 5% FBS, 0.5 % PenStrep) until 48 h. Cells were stained with H33342 and PI (both 0.25 µg/mL) and analyzed by fluorescence microscopy on a high-content microscope (In Cell Analyzer 2200) for GFP knockdown (described in high content imaging section below).

Gel permeation chromatography (GPC) analyses. Molecular weights (Mn) and molecular weight distributions (Mw/Mn) of selected polymers were measured by GPC on a HPLC Agilent 1260 system equipped with a guard column (Agilent, Aquagel, 10 mm, 10 µm) followed by three columns: (i)

Agilent, Aquagel-OH 40, 300 × 7.5 mm, 8 µm, (ii) Agilent, Aquagel-OH 50, 300 × 7.5 mm, 8 µm and (iii) Phenomenex, Polysep-GFC-P2000, 300 × 7.8 mm, range 100 – 10 k Da, connected to a UV (254 and 280 nm) and RI detector (Agilent). The GPC eluent was acetate buffer (0.5 mol/L, pH = 4.5), and the polymers were eluted at 0.7 mL/min. The temperature was set at 35 °C. Polyethylene oxide standards (EasyVial PEG/PEO, range 194 – 1000 k Da) were used to calibrate the SEC, since it has been demonstrated that such eluent composition allows PEO to be a suitable calibration standard for poly(amido amines).[1]

NP library preparation. Nanoparticle library was prepared in sterilized 96-deepwell plates by precipitation 15 µL of each polymer in water (960 µL, molecular biology grade, Fisher Bioreagents) and further addition of 25 µL of zinc sulfate (1M, Sigma-Aldrich). Plates were sealed with PP adhesive seals and left stirring on an orbital shaker (250 rpm) at 25 ºC. After a step of purification (centrifugation at 4 ºC, 8000 g for 8 min), the samples were resuspended in water (molecular biology grade) and lyophilized to determine the mass concentration of each nanoparticle. The efficiency of NP formation was calculated according to equation:

$$NP\ formation\ efficiency\ (\%) = \frac{M_{NP}}{M_{polymer}} \times 100$$

where M_{NP} denotes the weight of material recovered after NPs purification and freeze-drying and $M_{polymer}$ is the theoretical polymer weight.

Characterization of NP size and zeta potential. The diameter and zeta potential of NPs was measured by photon correlation spectroscopy (PCS) using quasi-elastic light scattering equipment (ZetaPALS analyser, Brookhaven Instruments Corp., Holtsville, NY) and ZetaPlus™ Particle Sizing Software (version 4.03). The scattered light was collected at fixed angle of 90º. To measure NPs size, a suspension of NP in water (molecular biology grade) was added to a cuvette (50 µg/mL, 2 mL), allowed to stabilize for 10 minutes and then analyzed at room temperature (3 times). To assess the percentage of NPs disassembly upon UV light irradiation (10 min, 365 nm, 100 mW/cm^2), a duplicate

of the samples was used and the values of NP diameter and NP counts (Kcps) were recorded. The zeta potential of NPs was determined in a 1 mM KCl solution at 25 ºC (50 μg/mL, 2 mL). All data were recorded as the mean of 5 measurements runs.

TEM analyses. The analysis was carried out on a FEI-Tecnai Spirit BioTwinG2 electron microscope. Aqueous dispersion of C11 NPs (500 μg/mL) was added on the surface of carbon coated 200 mesh copper grid and left air-dry for 5 h at room temperature in a closed petri dish. Digital images were acquired with coupled side mounted CCD camera MegaView III-SIS and the diameter of NPs was analysed with the Particle Tool from ImageJ.

High-throughput complexation of siRNAs with NPs. In a 96-deepwell plate, the NPs (50 μL, 400 μg/mL) were complexed with siRNA against eGFP (50 μL, 4 μg/mL siRNA and 4 μg/mL Cy5-tagged siRNA, GFP Duplex I, GE Dharmacon) at a weight ratio 1:50 (siRNA:NP). As control for siRNA activity and transfection, the same procedure was followed for lipofectamine RNAiMAX (15 μL/mL; Invitrogen). The plates were sealed (PP seals) and allowed to incubate at room temperature for 2 h on an orbital shaker (250 rpm). Samples were then diluted 1:10 with DMEM to 20 μg/mL NP concentration and directly used for cell transfection or determination of complexation efficacy. Complexation efficacy was determined indirectly from Cy5 tagged-siRNA after separating NPs and non-complexed siRNA by centrifugation (4ºC, 14.000g, 15 min), quantifying Cy5 fluorescence in three replicates of the supernatant. Concentration of siRNA was determined relative to a standard curve.

High-throughput transfections with NP@siRNA. Stable transfected HeLa-GFP (CellBiolabs Inc.) reporter cells were cultured in DMEM (without phenol red) containing FBS (10%, v/v), PenStrep (0.5%, v/v, 50 μg/mL) and blasticidin (10 μg/mL). 24 hours prior to the experiment, HeLa-GFP cells were seeded in 96 well plates (Costar) with a density of 4.000 cells per well. NP@siRNA complexes

(20 μg/mL) or lipofectamine RNAiMAX (1.5 μL/ml) were prepared in DMEM as described above. Cell transfections were performed with three technical replicates and plates in duplicate. After 10 min of cell material contact for transfection, medium was replaced by DMEM containing 5% FBS (v/v), PenStrep (0.5%, v/v, 50 μg/mL) and blasticidin (10 μg/mL). One plate duplicate was used for activation of the NP using a transilluminator (10 min, 365 nm, UVP BioSpectrum 500). The second plate of the duplicate (with same sample layout) remained without NP activation, allowing comparison of the bioactivity of released siRNA with and without activation by the light trigger. 48 h post transfection, cells were stained and placed in an automated incubator (Cytomat 2, Thermo) for high-content imaging analysis with an automated fluorescence microscope (In Cell 2200, GE Healthcare).

High-content imaging analyses. To distinguish viable cells from dead cells, cell nuclei were stained with Hoechst 33342 (Sigma-Aldrich, 0.25 μg/mL) and propidium iodide (PI, Sigma-Aldrich, 0.25 μg/mL). Dead cell nuclei are permeable for PI and show staining for H33342 and PI, where live cells are stained only with H33342. 48 h and 72 h post transfection, cells were analyzed on a high-content microscope (In Cell 2200, GE Healthcare) with a 20× objective, where 4 random image fields per well were imaged. Image analysis was performed with In Cell Developer software (GE Healthcare), applying machine learning algorithms. H33342 staining was used for definition of a nuclear mask (nuclei). Dead cell masks, with PI and H33342 staining overlapping 10% (dead nuclei) were subtracted from H33342 nuclear mask, resulting in viable nuclear population (viable nuclei). That mask was then dilated to cover as much of the cell region possible (cell). Next, nuclear mask was subtracted from the cell mask, resulting in a ring that masks the cytoplasm. GFP fluorescence intensity was measured in that cytoplasm mask of live cells. GFP knockdown was calculated as percentage of fluorescence on non-treated HeLa-GFP cells (after subtracting HeLa cell fluorescence background). From the difference of the total count of nuclei and dead nuclei count, cell viability was

calculated. By quantification of the Cy5 tagged siRNA in the cytoplasm, internalization of the NP was quantified.

siRNA release from C11 NPs after UV light irradiation. The release of siRNA from C11 (50 μg/mL, weight ratio 1:50 siRNA:NP, molar ratio 1:58 siRNA:NP) after UV-irradiation (10 min, 365 nm, 1 mW/cm^2) was determined by quantification of Cy5 tagged-siRNA in the supernatant after centrifugation (4ºC, 14000g, 15 min). The concentration of siRNA-Cy5 was determined by fluorescence in a microplate reader (Synergy H1) relative to a standard curve ($y = 3978.3x – 61.87$; $R^2 = 0.9869$).

Cellular internalization profiling of NPs. Human dermal keratinocytes (HaCaT cells; CLS Cell Lines Service GmbH, Eppelheim, Germany), human normal dermal fibroblast (NHDF) or human umbilical vein endothelial cells (HUVEC, Lonza) were used to quantify internalization of NP@siRNA complexes by colocalization with the endolysosomal compartment. HaCaT and NHDF cells were cultured in DMEM medium, HUVECs were cultured in EGM-2 medium (Lonza). All media was supplemented with FBS (10%, v/v) and PenStrep (0.5%, v/v, 50 μg/mL). Twenty-four hours prior to the experiment, cells were seeded to each well in black glass bottom 96 well plates (IBIDI, Germany) coated with 0.1% gelatine (Sigma) with densities of HaCaT and HUVECs at 20.000 cells/well, NHDF cells at 10.000 cells/well. Cells were stained with CellTrace™ CFSE 488 (5 μM; Molecular Probes, Life Technologies) according to manufacturer's instructions prior to the experiment. For cell transfection, cells were incubated for 1 h with NP@siRNA-Cy5 or lipofectamine@siRNA-Cy5 complexes in DMEM or EGM-2 media. Lysotracker Red (100 nM; Molecular Probes, Life Technologies) staining was added for 30 min during cell transfection. Next, complexes were removed, and cells were washed twice with PBS. After fixation with 4% (v/v) paraformaldehyde (Alfa Aesar) in PBS for 10 min at room temperature, cell nuclei were stained with

H33342 (2 μg/mL) for 10 min and subsequent washes with PBS. Cells were analysed by confocal microscopy (Zeiss LSM710) using a 40× immersion oil objective with two technical replicates per condition and a minimum of four representative image fields per replicate. Colocalization of NP@siRNA-Cy5 with Lysotracker red was analysed using JaCoP on ImageJ.

Complexation of PHD2 to the NPs. The complexation of PHD2 (GE Dharmacon) to C11 NPs followed the same procedure previously described for siRNA. Briefly, PHD2 and C11 NPs were mixed in molecular grade nuclease free, sterile water (Fisher Bioreagents) in a ratio of 1:50 (w/w, siRNA to NPs), and the suspension agitated on an orbital shaker for 2 h at room temperature. After complexation, the NP suspension was suspended in cell culture medium before use.

Proliferation of endothelial cells. To assess cell proliferation, EOMA-GFP cells cultured in DMEM medium containing FBS (10%, v/v) and PenStrep (0.5%, v/v, 50 μg/mL), were seeded in 24 well plates (7.500 cells/well; pre-coated for 10 min with 0.1% gelatine) and allowed to adhere overnight. Cells were transfected with C11@PHD2 complexes (20 μg/mL) for 12 h in DMEM with reduced FBS (2.5%, v/v and PenStrep). We have chosen 12 h because shorter transfection times did not translate in measurable functional activity (data not shown). Non-internalized NPs were removed, and medium was replaced by complete medium with 10% FBS (v/v) and PenStrep. NPs were activated with UV light, using a transilluminator (365 nm, 10 min, 1 mW/cm^2; UVP BioSpectrum 500). Cell growth was analyzed at 36 h post transfection by staining the cells with H33342 (1 μg/mL, Sigma) and fluorescence imaging (In Cell 2000). Nuclei were counted from H33342 nucleus staining on In Cell Developer. Each experimental condition was performed with at least three technical replicates. Six images per well were analyzed.

***In vitro* wound healing assay.** EOMA-GFP cells (15.000 cells/well) were seeded in 96 well plates (pre-coated for 10 min with 0.1% gelatine) 24 h prior to experiment to allow cells to grow to a complete monolayer in full medium (DMEM with FBS (10%, v/v) and PenStrep (0.5%, v/v, 50 µg/mL)). Cells were then inhibited by mitomycin (5 µg/mL, in cell culture medium, Tocris Bioscience) for 2 h and then transfected for 12 h with C11@PHD2 NPs (20 µg/mL) in DMEM with FBS (2.5%, v/v) and PenStrep (0.5%, v/v, 50 µg/mL). We have chosen 12 h because shorter transfection times did not translate in measurable functional activity (data not shown). NPs were then removed from the cells and washed with PBS. The monolayer was wounded, by scratching the cells with a yellow (200 µL) pipette tip. Cell debris and detached cells were removed by gently washes with PBS. Fresh medium (DMEM with FBS (1%, v/v) and PenStrep (0.5%, v/v, 50 µg/mL)) was added. NPs were then activated with UV light, using a transilluminator (365 nm, 10 min, 1 mW/cm^2; UVP BioSpectrum 500). Wound healing was monitored until 36 h post-scratch using brightfield microscopy (4x objective) on an automated microscope (In Cell 2000). Wound area was quantified by measuring cell free area with ImageJ. Relative wound closure was calculated at 36 h post wounding relative to time 0 h and normalized to control condition.

Quantitative analysis of PHD2 transfection by qRT-PCR. EOMA-GFP cells were seeded at 30.000 cells/well to 24 well plate pre-coated for 10 min with 0.1% gelatine. Cells were transfected for 12 h with C11-PHD2 (20 µg/mL) in DMEM with reduced FBS (2.5%, v/v) and PenStrep (0.5%, v/v, 50 µg/mL). Non-internalized NPs were removed by washing with PBS and further incubation with fresh medium (DMEM, 10% FBS, v/v 0.5% PenStrep). NPs were activated with UV light, using a transilluminator (365 nm, 10 min, 1 mW/cm^2; UVP BioSpectrum 500). After 24 h, cells from each condition were harvested after application of lysis buffer. RNA extraction was performed using RNeasy Plus Micro Kit (Quiagen) following manufacturers instruction. RNA was quantified on NanoDrop (Thermo Scientific). 1 µg total RNA was used to synthesize cDNA with qScript cDNA SuperMix (Quantabio). Quantitative RT-PCR was performed using NZYSpeedy qPCR Green Master

Mix (NZYTech, Portugal) on a RT-PCR (CFX Connect Real-Time System, BioRad). Quantification of the target gene (PHD2) was analyzed relative to GAPDH as housekeeping gene: $relative\ expression = 2^{[-(C_{T\ Sample} - C_{T\ GAPDH})]}$ (Supplementary Table 2). Minimal cycle threshold values (C_T) were calculated from at least 3 independent reactions. $\Delta\Delta C_T$ was calculated to determine relative PHD2 expression.

C11 NPs disassembly after UV light irradiation through a skin barrier. To demonstrate that NPs placed under a skin biopsy can be disassembled by UV light, a skin fragment (taken from the back of the mouse) was placed in a 1 cm^2 hole of a cardboard and a cuvette with a suspension of C11@siRNA (50 μg/mL) placed beneath the skin. The cuvette was irradiated with UV light (365 nm, 10 min, 1 mW/cm^2) and the number of NPs monitored by DLS. As control, a cuvette with C11@siRNA (50 μg/mL) was used in the same set up but without skin.

1. Xing, H.; Lu, M.; Xian, L.; Zhang, J.; Yang, T.; Yang, L.; Ding, P. *Asian Journal of Pharmaceutical Sciences* **2017,** 12, (3), 292-298.

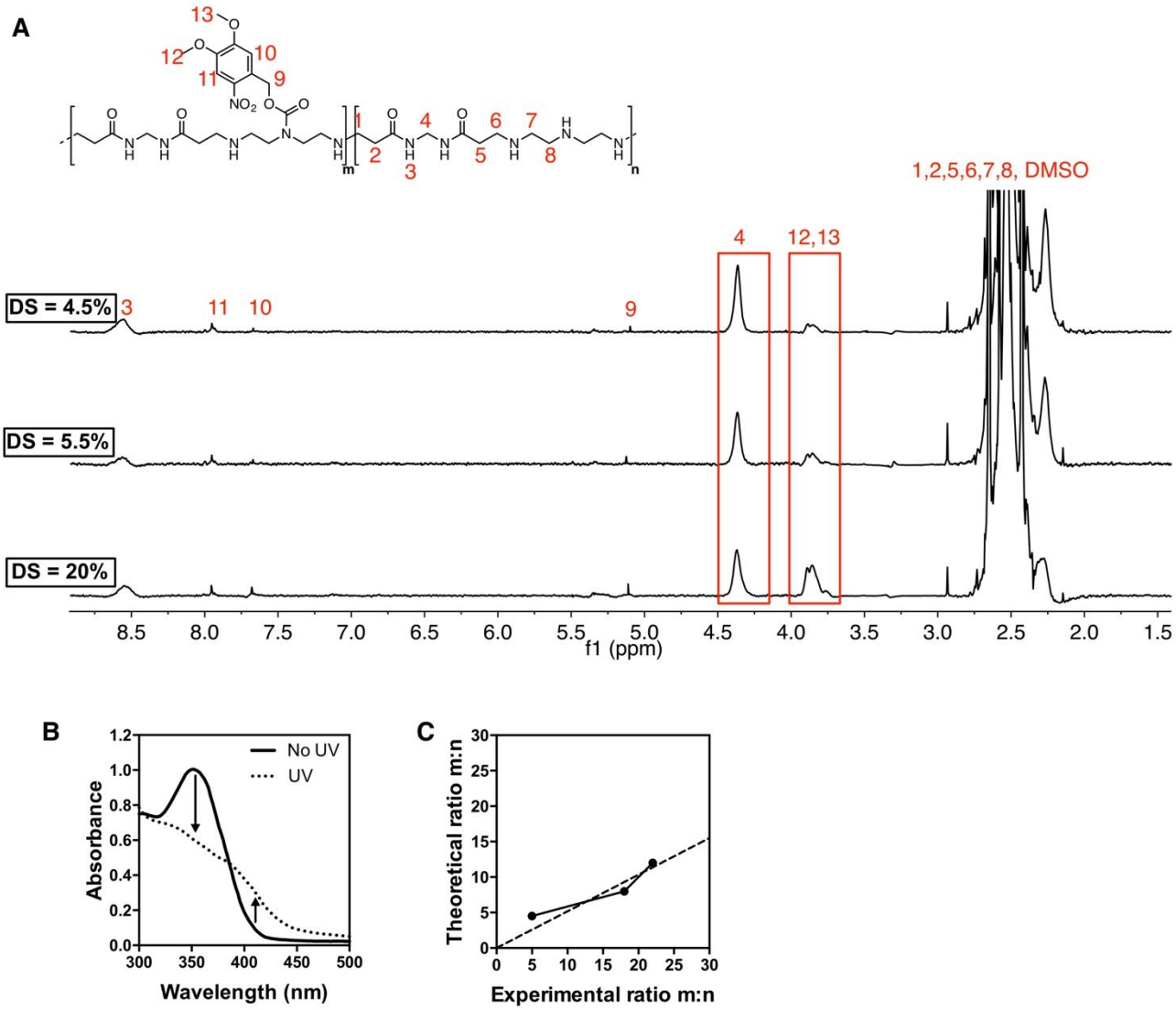

Figure S1. Optimisation of the light-cleavable moiety (NVOC) ratio in the polymer A4. After the synthesis, the polymer was reacted with NVOC at the following theoretical molar ratio (NVOC:diamine): 1:4, 1:8 and 1:12. To calculate the ratio of incorporation of NVOC into the polymer, polymers were precipitated in water, lyophilized, resuspended in DMSO-d_6 and analyzed by ^{1}H-NMR. (A) NMR spectra (in DMSO-d6) of A4 polymers with different NVOC-Cl:diamine molar ratios. The results show a degree of substitution of 20 %, 5.5% and 4.5%. (B) Effect of UV light (10 min, 365 nm, 200 mW/cm^2) in the absorbance of the polymer A4 (DS_{exp} = 20%). The decrease in absorption at 350 nm (NVOC) and the increase at 420 nm (nitroso product) indicate the photo-cleavage of NVOC. (C) Theoretical and experimental NVOC:diamine molar ratio´s ratio by NMR.

A

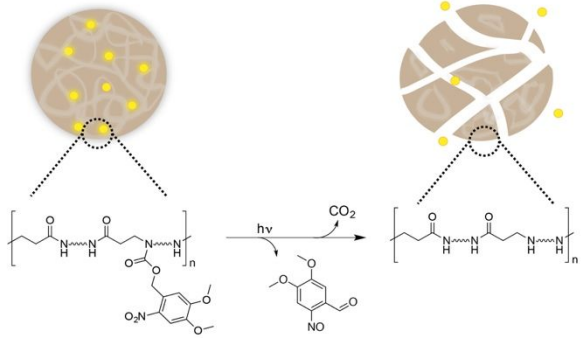

B

	UV	Diameter (nm)	Count (kcps)	C.decrease (%)
DS = 20%	No	165.7	124.0	87.7
	Yes	2.2	15.2	
DS = 5.5%	No	140.2	170.8	85.1
	Yes	176.1	25.4	
DS = 4.5%	No	306.8	230.5	80.8
	Yes	579.5	44.2	

Figure S2. (A) Schematic illustration of NPs disassembly upon UV light irradiation. (B) Optimisation of the NVOC to amine ratio in the nanoparticle A4, to obtain the higher nanoparticle count decrease after UV irradiation. The formulation (50 μg/mL) was irradiated with UV light (365 nm, 200 mW/cm^2) for 10 min.

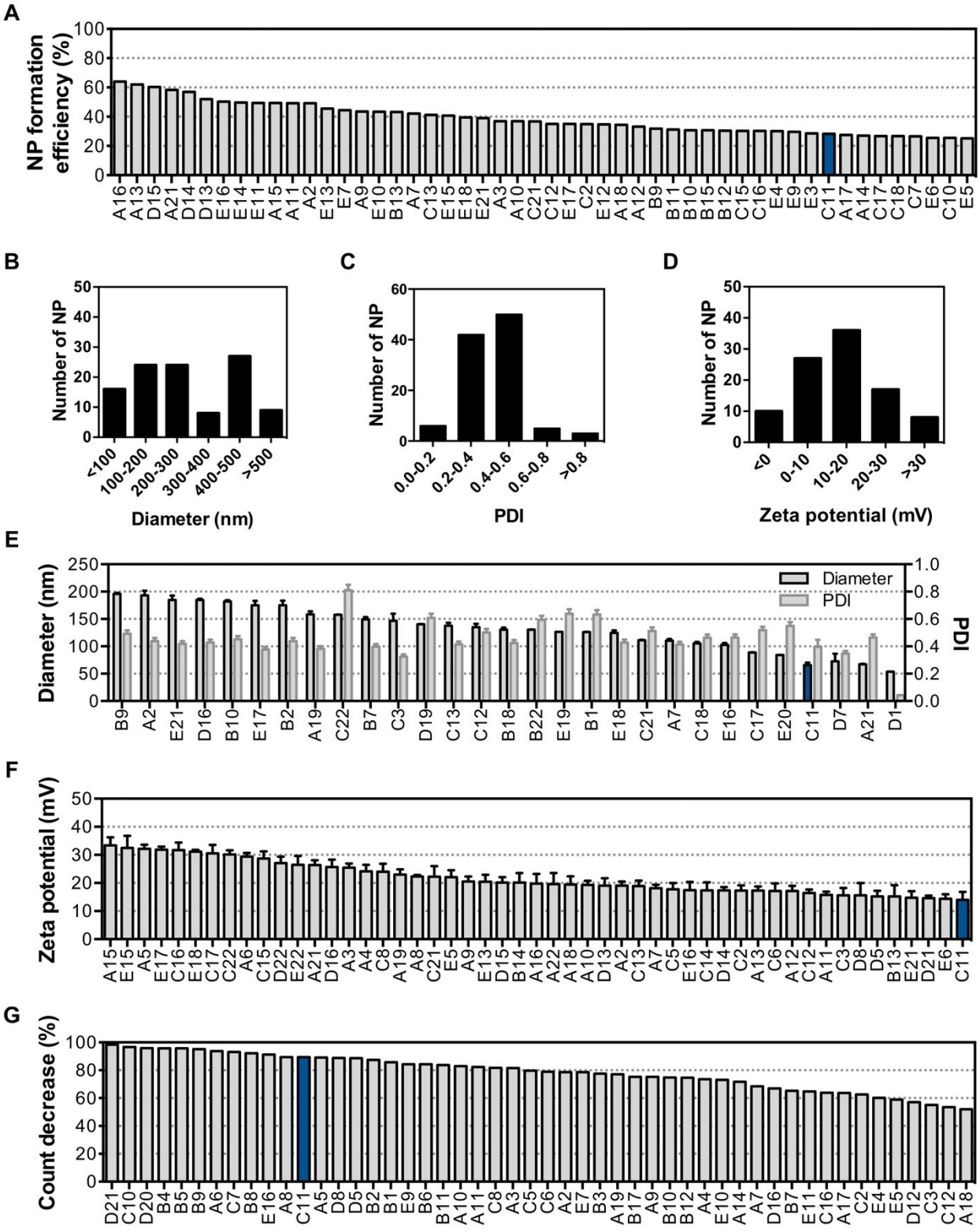

Figure S3: Physicochemical properties of the 50 top NP formulations. (A) Efficiency of NP formation calculated from the ratio of theoretical polymer weight and weight of NP after purification. (B) Diameter frequency distribution. (C) PDI frequency distribution. (D) Zeta potential frequency distribution. (E) Size and PDI of nanoparticles within size range between 50 and 200 nm. (F) Zeta potential of the NPs measured by DLS. In E and F, results are Mean ± SEM (n = 3). (G) NP disassembly by light. Count decrease was determined by DLS after 10 min UV irradiation (365 nm, 200 mW/cm^2).

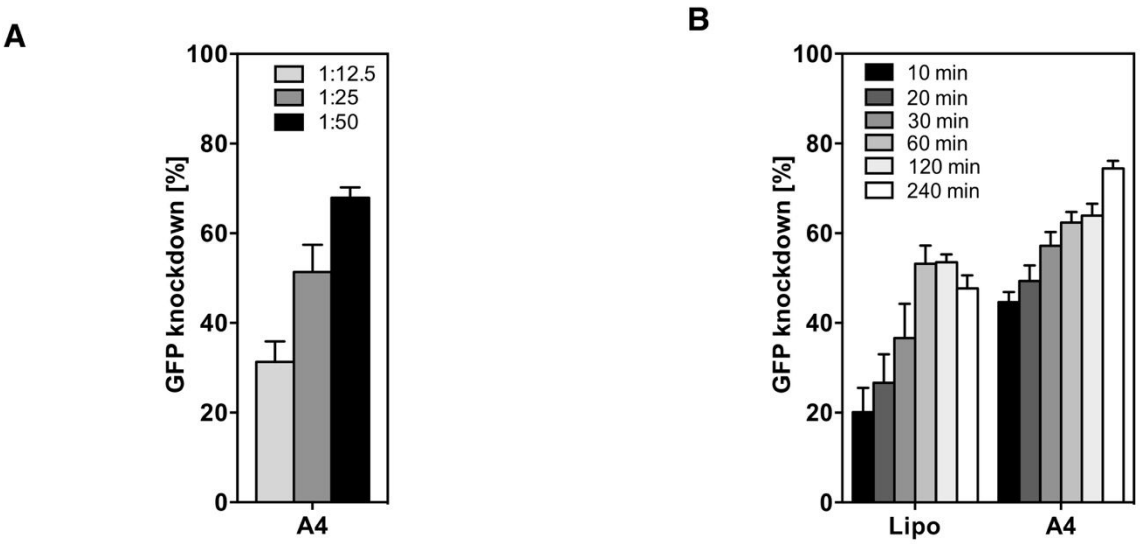

Figure S4. Evaluation of siRNA:NP ratio and transfection time in the knock down efficiency of the formulations. (A) Effect of the ratio siRNA:NP in the knock down efficiency. HeLa-GFP cells were transfected for 4 h with a NP formulation (formulation A4; 20 μg/mL) containing a siRNA-Cy5 against GFP at different ratio´s siRNA:NP (1:12.5; 1:25 and 1:50, w/w). GFP knockdown was quantified at 48 h post transfection. (B) Effect of transfection time in the knock down efficiency. Cells were transfected for various times (between 10 and 240 min) with A4 NP@siRNA-Cy5 complexes (20 μg/mL; 1:50 siRNA:NP, w/w). Lipofectamine RNAiMAX (Lipo) was used as a control transfection agent. GFP knockdown was analysed at time 48 h after transfection by high content microscopy. All results are presented as Mean ± SEM (n = 3).

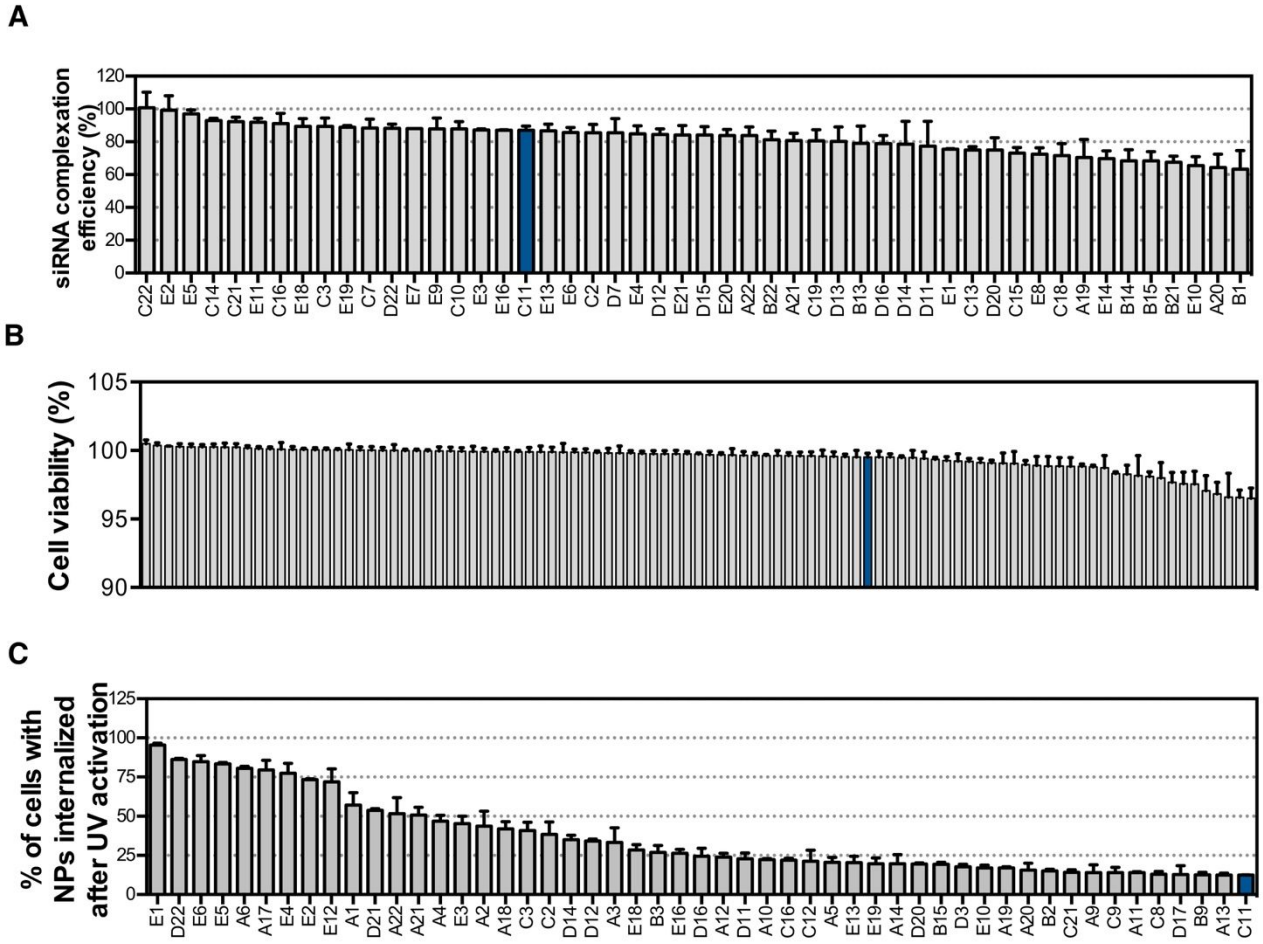

Figure S5. Complexation capacity of the NPs for siRNA as well as cytotoxicity and cellular internalisation of NP@siRNA complexes. NPs complexed with siRNA (siRNA:NP ratio = 1:50, w/w) were used for toxicity and cell internalisation studies (in HeLa cells). The concentration of NPs@siRNA-Cy5 was 20 μg/mL and the transfection time of 10 min. (B) Efficiency of siRNA complexation in the top 50 formulations. (B) Cell viability at 48 h post transfection without UV irradiation. Cell nuclei were stained with Hoechst H33342 and dead cells with propidium iodide. Cell viability was calculated as the % of dead nuclei from the total count of nuclei. (C) Percentage of cells stained for NPs@siRNA-Cy5 (siRNA:NP ratio = 1:50, w/w) at 48 h post-transfection. The graph shows the top 50 NP formulations with high cell internalization. In A, B and C, results are Mean ± SEM (n=3).

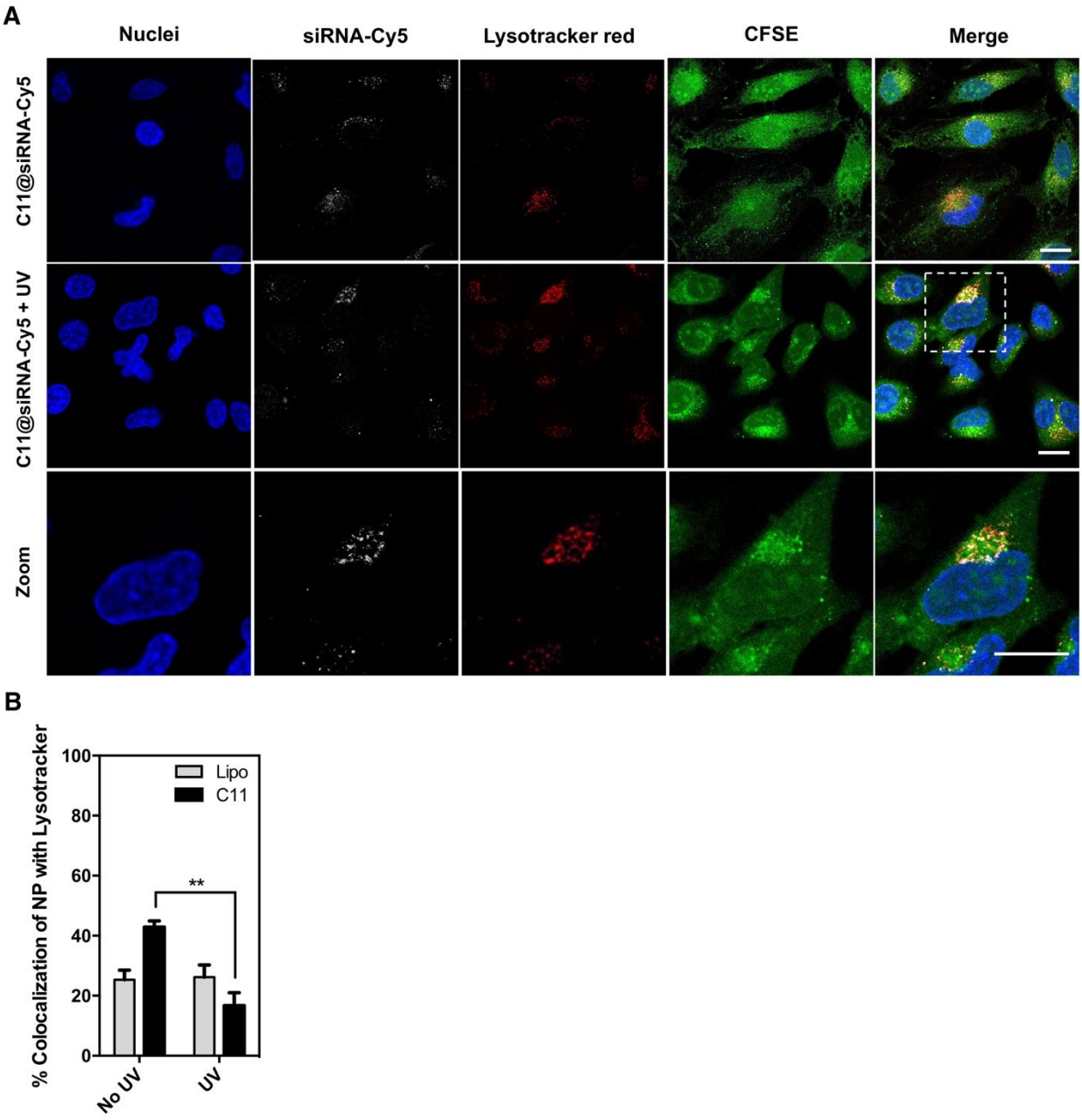

Figure S6. C11@siRNACy5 colocalization with LysoTracker Red. HeLa cells were transfected with C11@siRNA-Cy5 (20 µg/ml) or Lipo@siRNA-Cy5 for 10 minutes. Cells were then washed and NPs were activated with UV light (10 min, 1 mW/cm^2). The cells were stained with CFSE for cell membrane, LysoTracker red for endolysosome, H333342 for cell nuclei and analysed 1 h after transfection by confocal microscopy. (A) Representative confocal microscopy images showing the colocalization of C11@siRNA-Cy5 formulation irradiated or not with UV light with Lysotracker Red. White scale bar is 20 µm. (B) Colocalization of Lysotracker Red with siRNA-Cy5 expressed as the Manders' overlap coefficient quantified using JACoP on ImageJ. Results are resented as Mean ± SEM. Statistical analysis was assessed by unpaired student t-test with Welch's correction. ** P <0.01.

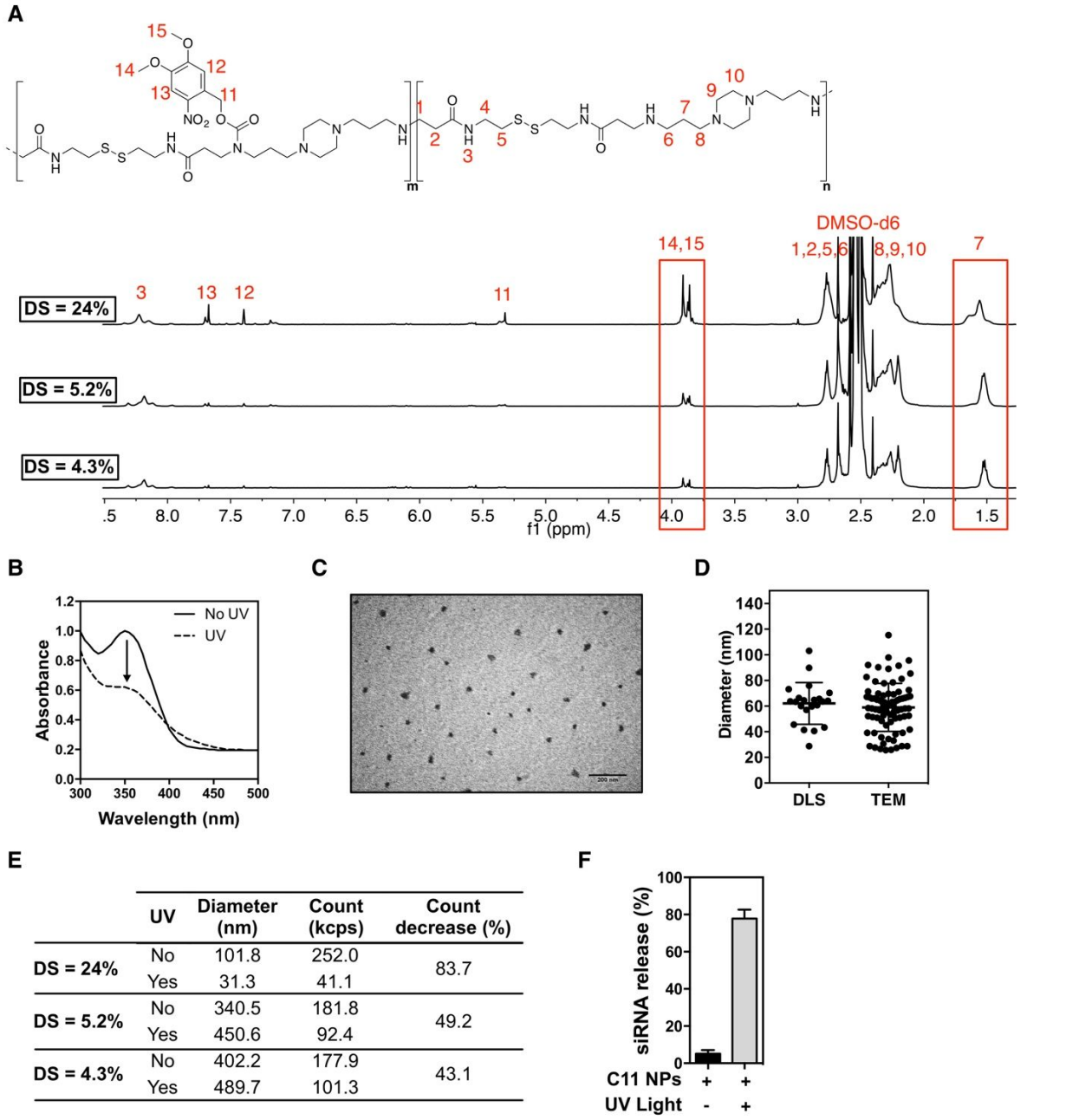

	UV	Diameter (nm)	Count (kcps)	Count decrease (%)
DS = 24%	No	101.8	252.0	83.7
	Yes	31.3	41.1	
DS = 5.2%	No	340.5	181.8	49.2
	Yes	450.6	92.4	
DS = 4.3%	No	402.2	177.9	43.1
	Yes	489.7	101.3	

Figure S7. Characterization of C11 polymer and NPs. (A) NMR spectra (in DMSO-d6) of C11 polymers with different NVOC:diamine molar ratios. The results show a DS_{exp} of 24.0 %, 5.2% and 4.3% (DS_{theo} = 25%, 12.5% and 8.3%, respectively). (B) Effect of UV light (10 min, 365 nm, 200 mW/cm^2) in the absorbance of the polymer C11 (DS_{exp} = 24%). The decrease in absorption at 350 nm (NVOC) and the increase at 420 nm (nitroso product) indicate the photo-cleavage of NVOC. (C) Representative image of NPs obtained by TEM (DS_{exp} = 24%). Bar corresponds to 200 nm. (D) Distribution of NP diameters as evaluated by TEM and DLS analyses. For DLS analyses, a suspension of NPs at a concentration of 50 µg/mL was used. For TEM analyses, a NP suspension at a concentration of 500 µg/mL was applied on carbon coated 200 mesh copper grids, left to air dry and analyzed (FEI-Tecnai Spirit BioTwinG2). The images were acquired and analysed on ImageJ. Results are Mean ± SEM (n = 2-5, up to 5 images per replicate). (E) Disassembly of C11 NPs with different ratios of NVOC after UV irradiation. The formulations (50 µg/mL) were irradiated with UV light (365 nm, 10 min, 200 mW/cm^2) for 10 min and analysed by DLS. (F) siRNA-Cy5 release from C11 NPs (50 µg/mL) after UV light irradiation (10 min, 1 mW/cm^2). siRNA-Cy5 was determined in the supernatant relative to a standard curve. Results are presented as Mean ± SEM (n = 3).

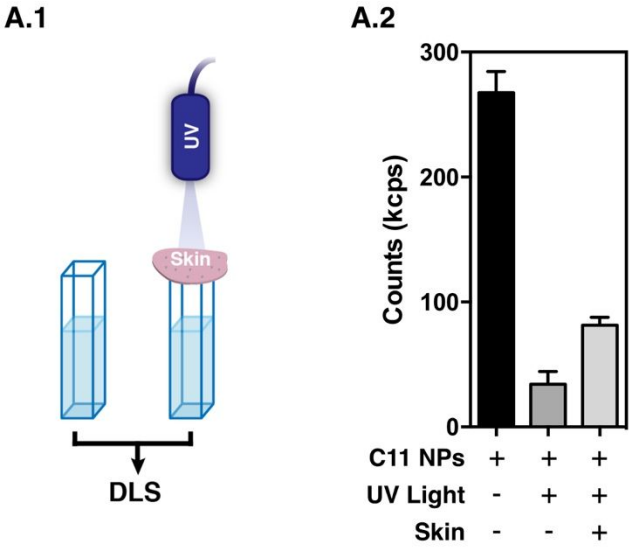

Figure S8. Photo-disassembly of C11@siRNA NPs. (A.1) Schematic representation of the methodology used to evaluate the photo-disassembly of C11@siRNA NPs beneath a mouse skin biopsy. A skin fragment (diameter ~1.7 cm placed on a cardboard with a 1 cm^2 hole; thickness of 200-230 µm as measured by a caliper) was placed above a cuvette containing a suspension of C11@siRNA (50 µg/mL, 2 mL). The cuvette was irradiated with UV light at 1 mW/cm^2 during 10 min and then analysed by DLS to determine NP count (A.2). In A.2, results are presented as Mean ± SEM (n = 3).

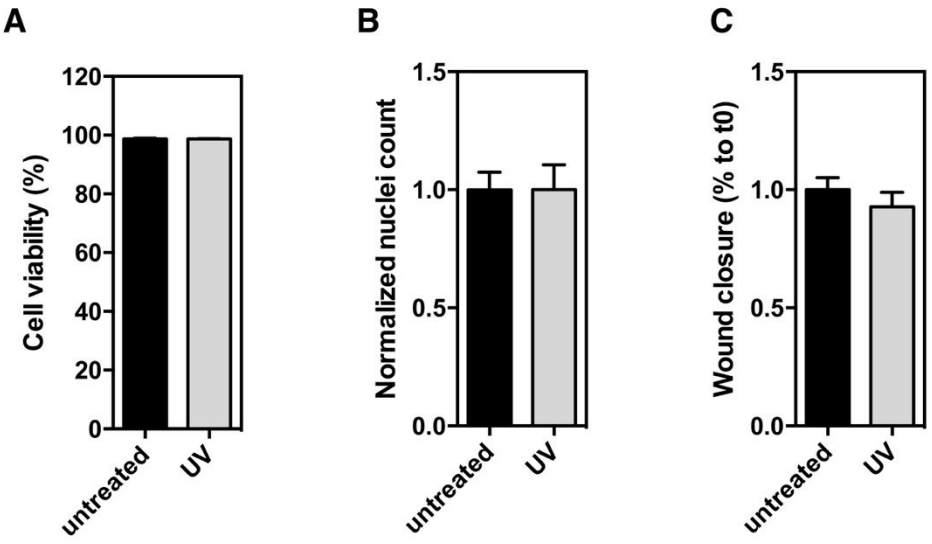

Figure S9. Influence of UV light on cell viability and activity. Cells were irradiated or not with UV light (10 min, 1 mW/cm^2) and analysed at 48 h. (A) Cell viability of HeLa-GFP cells. Cell nuclei were stained with Hoechst H33342 and propidium iodide at 48 h, and cell viability calculated as the % of dead nuclei from the total count of nuclei. (B) Endothelial cell proliferation. Nuclei were stained with H33342 and analysed by high content imaging at time 48 h. The number of cells at time 48 h was normalized by the one at time 0. (C) Endothelial cell migration. Wound area was quantified in ImageJ and normalised to the initial wound area. All results are presented as Mean ± SEM (n = 3).

Supplementary Table 1. Detailed description of name, CAS, Vendor, structure of library monomers

Monomer	Chemical Name IUPAC	CAS	Vendor
A	Methylenebisacrylamide	110-26-9	Aldrich
B	Hexamethylenebisacrylamide	16069-15-1	Aldrich
C	Cystaminebisacrylamide	6098-457-8	Polyscience
D	Dihydroxyethylenebisacrylamide	868-63-3	Aldrich
E	Bisacryloylpiperazin	6342-17-2	Sigma
1	Ethylenediamine	107-15-3	Merck
2	1,4-Diaminobutan	110-60-1	Aldrich
3	1,6-Diaminohexan	124-09-4	Alfa Aesar
4	Diethylenetriamine	111-40-0	Alfa Aesar
5	Triethylenetetraamine	112-24-3	Acros Organics
6	Pentaethylenehexamine	4067-16-7	Aldrich
7	3,3'-Diamino-N-methyldipropylamine	105-83-9	Aldrich
8	1,2-Diaminocyclohexane	694-83-7	Aldrich
9	1,8-Diamino-3,6-dioxaoctane	929-59-9	Acros Organics
10	1,13-Diamino-4,7,10-trioxatridecane	4246-51-9	Aldrich
11	1,4-Bis(aminopropyl)piperazine	7209-38-3	Aldrich
12	1,4-Phenylenedimethanamine	539-48-0	Merck
13	1,5-Diaminonaphthalene	2243-62-1	Aldrich
14	4,4'-methylenedianiline	101-77-9	Aldrich
15	1,3-Phenylenediamine	108-45-2	TCI Chemicals
16	1,3-Diaminopropane	109-76-2	TCI Chemicals
17	2,2-Dimethyl-1,3-propanediamine	7328-91-8	TCI Chemicals
18	1,3-Diaminopentane	589-37-7	TCI Chemicals
19	2,2'-Diamino-N-methyldiethylamine	4097-88-5	TCI Chemicals
20	Agmatine sulfate	2482-00-0	TCI Chemicals
21	1,4-Bis(aminomethyl)cyclohexane	2579-20-6	TCI Chemicals
22	4,4'-Methylenebis(cyclohexylamine)	1761-71-3	Aldrich

Supplementary Table 2. Sequence of primers used in qRT-PCR experiments.

Gene		Sequence	species
m-PHD2	FW	CCACTGGCACTCAACTAACTCA	mouse
	RW	CCGAGTTCATTTAGTGCCCGTCA	
m-GAPDH	FW	AAGGTCATCCCAGAGCTGAA	mouse
	RW	CTGCTTCACCACCTTCTTGA	